Journal of ELECTRONIC MATERIALS, Vol. 47, No. 3, 2018
https://doi.org/10.1007/s11664-017-5999-2

Impact Factors Analysis of the Hot Side Temperature of Thermoelectric Module

XINGYU ZHANG,[1,2,3] GANGFENG TAN,[1,2] and BO YANG[1,2,4]

1.—School of Automotive Engineering, Wuhan University of Technology, Wuhan 430070, China. 2.—Hubei Key Laboratory of Advanced Technology for Automotive Components, Wuhan University of Technology, Wuhan 430070, China. 3.—GEELY Automobile Research Institute, Ningbo 315000, China. 4.—e-mail: yangbo92@126.com

The thermoelectric generator (TEG) plays a crucial role in converting the waste energy of exhaust into electricity, which ensures energy saving and increased fuel utilization efficiency. In the urban driving cycle, frequent vehicle operation, like deceleration or acceleration, results in continuous variation of the exhaust temperature. In order to make the operating performance stable, and to weaken the adverse effects of the frequent variation of the exhaust temperature on the lifetime and work efficiency of the electronic components of TEG systems, the output voltage of the thermoelectric (TE) module should stay more stable. This article provides an improved method for the temperature stability of the TE material hot side based on sandwiching material. From the view of the TEG system's average output power and the hot side temperature stability of the TE material, the analyzing factors, including the fluctuation frequency of the exhaust temperature and the physical properties and thickness of the sandwiching material are evaluated, respectively, in the sine and new European driving cycle (NEDC) fluctuation condition of the exhaust temperature. The results show few effects of sandwiching material thickness with excellent thermal conductivity on the average output power. During the 150–170 s of the NEDC test condition, the minimum hot side temperatures with a BeO ceramic thickness of 2 mm and 6 mm are, respectively, 537.19 K and 685.70 K, which shows the obvious effect on the hot side temperature stability of the BeO ceramic thickness in the process of acceleration and deceleration of vehicle driving.

Key words: TE material, sandwiching material, hot side temperature stability, output power

INTRODUCTION

With the urgent demand for electricity, sustainable energy technologies are the focus in energy utilization.[1–3] Currently, the renewable energy sources (solar, wind, and geothermal) account for a small fraction of the electricity consumed, which has not affected the relatively high costs of energy utilization. Therefore, it is significant to find cost-effective technologies for generating electricity from waste heat.[4] Although thermoelectric (TE) technologies are not likely to replace the conventional Stirling or Rankine cycle steam engines in the near future, thermoelectric generators (TEG) with low cost can achieve the direct conversion of heat into electricity, especially for waste heat recovery.[5] Nowadays, researchers study the thermoelectric technology for the achievement of high-energy conversion efficiency and cost/efficiency balance.[6–10] In general, only 30% of an engine's fuel combustion energy is converted into useful work, and nearly 40% of heat energy is wasted with the engine exhaust gas.[11] Low-grade waste heat recovery technology in vehicles mainly includes the Organic

(Received June 1, 2017; accepted December 1, 2017; published online December 12, 2017)

Rankine Cycle and TEG technology. Furthermore, the maximum utilization of waste heat recovery is essential.[12–14]

In hilly ground, when the vehicle works with a stable speed and fixed gears, the exhaust temperature will fluctuate drastically on different road slopes and the exhaust mass flow rate maintains a stable value.[15] The fluctuating conditions of the hot side of the TE module will lead to instability and low efficiency of the TEG system. The key to this problem is to delay the temperature fluctuation of the hot side. The asynchronous temperature characteristic of the exhaust and the hot side of the TE material can be decided by the physical properties of the sandwiching material.

McCarty took an experimental setup composed of a fixed heat source and a variable thermal resistance air gap serving as a thermal switch to improve the output power ratio through the TE device.[16,17] Gou developed a novel TEG system with a thermal switch to solve the temperature fluctuation problem proposed by McCarty.[18] However, the complexed device with a variable air gap between the heat source and TE materials is unsuitable when installed in a vehicle exhaust pipe.

In order to investigate the temperature reduction of TE material along the x position, the state–space expression of the dynamic heat transfer model in the transverse direction including the exhaust, sandwiching material, thermoelectric material and water are established through the energy conservation equation and the forward and backward differential methods. For explicitly studying the dynamic heat transfer process in the longitudinal direction, the key point focuses on the temperature iteration algorithms exhibited by the running diagram and the solving method of the contact surface temperature of the sandwiching and TE material. From the point of view of the average output power and the hot side temperature stability of TE material, the analyzing factors, such as the fluctuation frequency of the exhaust temperature and the physical properties and thickness of the sandwiching material are evaluated, respectively, in the sine and new European driving cycle (NEDC) fluctuation condition of exhaust temperature. To keep the hot side temperature stable and acquire higher generation power for thermoelectric modules, the analysis provides a method for choosing the applicable sandwiching material.

MATHEMATICAL MODEL

Basics of TEG

As illustrated in Fig. 1, in the schematic diagram of a typical thermoelectric power generation system, a series of TEG legs are connected electrically in series via copper strip connectors. The heat from the exhaust flows through the ceramic plate, copper strip, TEG legs, copper strip, and ceramic plate, then reaches the water. In the process of energy transfer, a part of the heat is converted to electric power via the Seebeck effect of thermoelectric materials. Furthermore, the vast majority of the remaining heat is assimilated by the heat sink and dissipated into the atmosphere.[19–22]

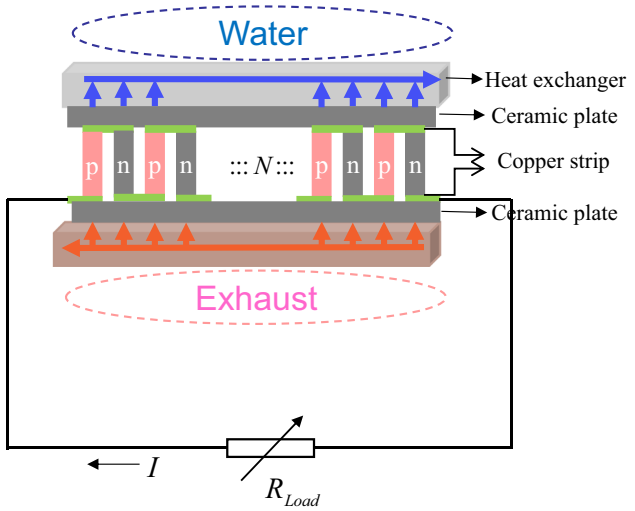

Fig. 1. Schematic diagram of a typical TEG system.

Heat Transfer Model in x Direction

For clearly demonstrating the physical model with several assumptions, the simplified model in the x direction is shown in Fig. 2. In the simplified physical model, the ceramic plate is replaced by the sandwiching material. A kind of heat convection generates between the water and the TE material, and the another is produceds between the exhaust and the sandwiching material. The wall of the thermoelectric material is divided into n equal parts along the x direction. For the element of volume, the energy conservation equation is applied in the cold fluid, exhaust, TE material, and sandwiching material. However, several assumptions must be put forward.

- The temperature of the cold fluid, while hot fluid only changes in the x direction, can be considered as a one-dimensional heat transfer model.
- Neglecting the influence of the copper strip.
- Assuming that the water is in direct contact with the TE material.
- The convective heat transfer coefficient is regarded as constant value along the flow direction.
- The thermal radiation of exhaust is neglected.
- The specific heat capacity and thermal conductivity of the TE materials are fixed.

For analyzing the dynamic heat transfer model in the x direction, the partial differential equations

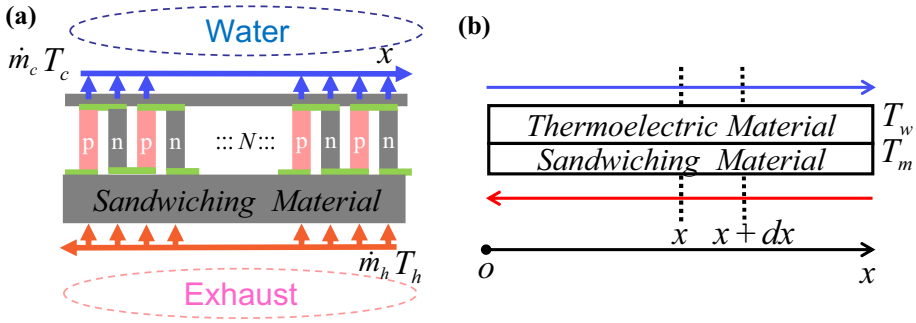

Fig. 2. The conceptual diagram (a) of the analysis model and the simplified model (b) in *x* direction.

(PDEs) of the water, exhaust, TE material and sandwiching material in time and space can be developed with the energy conservation equation in the d*x* section.

$$\frac{\partial T_{\mathrm{c}}}{\partial t} + C_{11}\frac{\partial T_{\mathrm{c}}}{\partial x} = C_{12}(T_{\mathrm{w}} - T_{\mathrm{c}}) \tag{1}$$

$$\frac{\partial T_{\mathrm{h}}}{\partial t} - C_{21}\frac{\partial T_{\mathrm{h}}}{\partial x} = C_{22}(T_{\mathrm{m}} - T_{\mathrm{h}}) \tag{2}$$

$$\frac{\partial T_{\mathrm{w}}}{\partial t} = C_{31}T_{\mathrm{c}} + C_{32}T_{\mathrm{m}} + C_{33}T_{\mathrm{w}} \tag{3}$$

$$\frac{\partial T_{\mathrm{m}}}{\partial t} = C_{41}T_{\mathrm{w}} + C_{42}T_{\mathrm{h}} + C_{43}T_{\mathrm{m}} \tag{4}$$

In Eqs. 1–4, the subscripts c, h, w and m represent the cold side, hot side, thermoelectric material, and sandwiching material, respectively; T indicates the node temperature in the *x* direction; $\dot{m}$ indicates mass flow; H and W are the thickness and the width of each layer; ρ and c represent the density and the specific heat capacity; h_{c} and h_{h} indicate the convective heat transfer coefficient in the cold side and hot side; h_{m} is the contact convective heat transfer coefficient between the TE material and the sandwiching material. Also, the coefficient in the equations can be solved (see supplementary data file).

The boundary conditions of the mathematic model describing the inlet temperature of the water and exhaust are shown as follows:

$$\begin{cases} T_{\mathrm{c}}(0,t) = T_{\mathrm{c,in}} \\ T_{\mathrm{h}}(L,t) = T_{\mathrm{h,in}} \end{cases} \tag{5}$$

where $T_{\mathrm{c,in}}$ and $T_{\mathrm{h,in}}$ indicate the entrance temperature ofthe water and exhaust, respectively.

The initial condition with original temperature is set as follows:

$$T_{\mathrm{c}}(x,0) = T_{\mathrm{h}}(x,0) = T_{\mathrm{w}}(x,0) = T_{\mathrm{m}}(x,0) = T_0 \tag{6}$$

Where T_0 represents the initial temperature; $T_{\mathrm{c}}(x, 0)$, $T_{\mathrm{w}}(x, 0)$, $T_{\mathrm{m}}(x, 0)$, and $T_{\mathrm{h}}(x, 0)$ indicate the nodes' temperature of the water, TE material, sandwiching material, and exhaust individually.

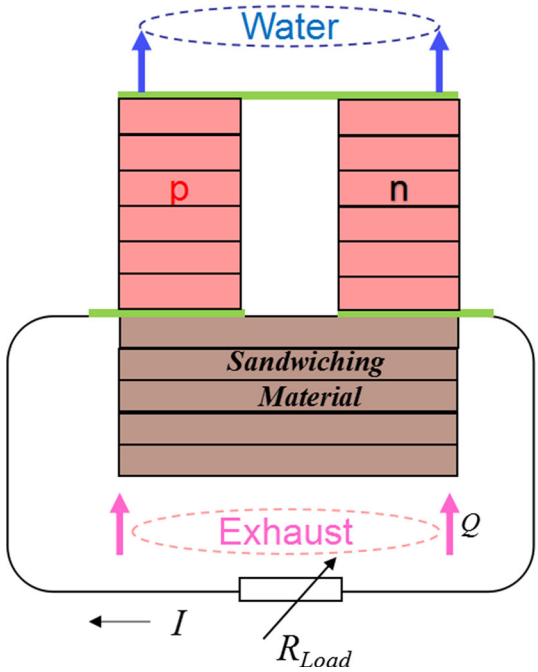

Fig. 3. Schematic view of a single TEG for finite element analysis.

Heat Transfer Model in *y* Direction

As illustrated in Fig. 3, in order to facilitate the finite element analysis, the TEG legs and sandwiching material are fractionally divided into isometric elements along the leg height of the TEG.[23–28] For the purpose of predigesting the model, the assembly with the TE material and sandwiching material is regarded as a composite wall.

On account of the conduction effect in the TE material, the process of heat conduction in the *y* direction can be presented by the partial differential form[29]:

$$\frac{\partial^2 T}{\partial y^2} = \frac{1}{\alpha_{\mathrm{w}}} \times \frac{\partial T}{\partial t} \tag{7}$$

$$\alpha_{\mathrm{w}} = \frac{k_{\mathrm{w}}}{\rho_{\mathrm{w}} c_{\mathrm{w}}} \tag{8}$$

where k_w indicates the heat conductivity coefficient of the TE material; and α_w is the thermal diffusion coefficient of the TE material.

Similarly, the course of the heat transfer in the sandwiching material in the y direction can be expressed as:

$$\frac{\partial^2 T}{\partial y^2} = \frac{1}{\alpha_m} \times \frac{\partial T}{\partial t} \tag{9}$$

$$\alpha_m = \frac{k_m}{\rho_m c_m} \tag{10}$$

where k_m is the heat conductivity coefficient of the sandwiching material; and α_m is the thermal diffusion coefficient of sandwiching material.

According to Fourier's law, the temperature gradient is mainly decided by the thermal conductivity of the material. As illustrated in Fig. 4, the static temperature of different nodes in the equivalent heat network can be expressed as follows.

$$\frac{T_{s,1} - T_h}{1/h_h} = \frac{T_{s,2} - T_{s,1}}{H_m/k_m} = \frac{T_{s,3} - T_{s,2}}{H_w/k_w} = \frac{T_c - T_{s,3}}{1/h_c} \tag{11}$$

Initial and Boundary Conditions

From Fig. 4, the boundary conditions of the exhaust can be illustrated as:

$$-k_w \frac{\partial T}{\partial y}\Big|_{y=0} = h_h[T_h - T_m(0,t)] \tag{12}$$

The boundary conditions of water can be exhibited as:

$$-k_w \frac{\partial T}{\partial y}\Big|_{y=L} = h_c[T_w(L,t) - T_c] \tag{13}$$

At the initial time in the y direction, the initial temperature of the material is expressed as:

$$T(y,0) = T_0 \tag{14}$$

The symbol of $T(y, t)$ indicates the temperature in position y and time t. The parameters of water, exhaust, TE material (Bi_2Te_3) and sandwiching (BeO ceramic) material are detailed in Tables I nd II.

FINITE ELEMENT ANALYSIS

Numerical Solving Method Along the *x* Direction

As the dynamic model of heat transfer involves time and space, the PDEs (Eqs. 1–4) can be discrete in space and time by the finite element method. The forward and backward differential methods are applied in Eqs. 1–4, respectively, as follows:

$$\frac{\partial T_c^{k+1}}{\partial t} = -\frac{C_{11}}{\delta x} \cdot T_c^{k+1} + \left(\frac{C_{11}}{\delta x} - C_{12}\right) T_c^k + C_{12} T_w^k \tag{15}$$

$$\frac{\partial T_h^{k-1}}{\partial t} = -\frac{C_{21}}{\delta x} \cdot T_h^{k-1} + \left(\frac{C_{21}}{\delta x} - C_{22}\right) T_h^k + C_{22} T_m^k \tag{16}$$

$$\frac{\partial T_w^k}{\partial t} = C_{31} T_c^k + C_{32} T_m^k + C_{33} T_w^k \tag{17}$$

$$\frac{\partial T_m^k}{\partial t} = C_{41} T_w^k + C_{42} T_h^k + C_{43} T_m^k \tag{18}$$

The differential equations can be transformed to a state–space expression as follows:

$$\begin{aligned}
&\left[\frac{\partial T_c^1}{\partial t} \quad \frac{\partial T_c^2}{\partial t} \quad \cdots \quad \frac{\partial T_c^n}{\partial t} \quad \frac{\partial T_h^0}{\partial t} \quad \frac{\partial T_h^1}{\partial t} \quad \cdots \quad \frac{\partial T_h^{n-1}}{\partial t} \quad \frac{\partial T_w^0}{\partial t} \quad \frac{\partial T_w^1}{\partial t} \quad \cdots \quad \frac{\partial T_w^n}{\partial t} \frac{\partial T_m^0}{\partial t} \frac{\partial T_m^1}{\partial t} \cdots \frac{\partial T_m^n}{\partial t}\right]^{\mathrm{T}} \\
&= \begin{bmatrix} [A] & [0] & [B] & [0] \\ [0] & [C] & [0] & [D] \\ [E] & [0] & [F] & [G] \\ [0] & [H] & [I] & [J] \end{bmatrix} \times \left[T_c^1 \quad T_c^2 \quad \cdots \quad T_c^n \quad T_h^0 \quad T_h^1 \quad \cdots \quad T_h^{n-1} \quad T_w^0 \quad T_w^1 \quad \cdots \quad T_w^n T_m^0 T_m^1 \cdots T_m^n\right]^{\mathrm{T}} \\
&\quad + [K] \times \left[T_c^0(t) \quad T_h^n(t)\right]^{\mathrm{T}}
\end{aligned} \tag{19}$$

where the left $(4n + 2) \times 1$ matrix represents the temperature derivative in each node, and the right 2×1 matrix indicates the boundary conditions of the water and exhaust. By the state–space block of Matlab/Simulink, the state variables of the transient temperature of nodes can be solved. In addition, the matrices of the state–space equation are demonstrated (see supplementary data file).

Numerical Solving Method Along the *y* Direction

Before establishing the analysis model of heat transfer in the y direction, it was assumed the

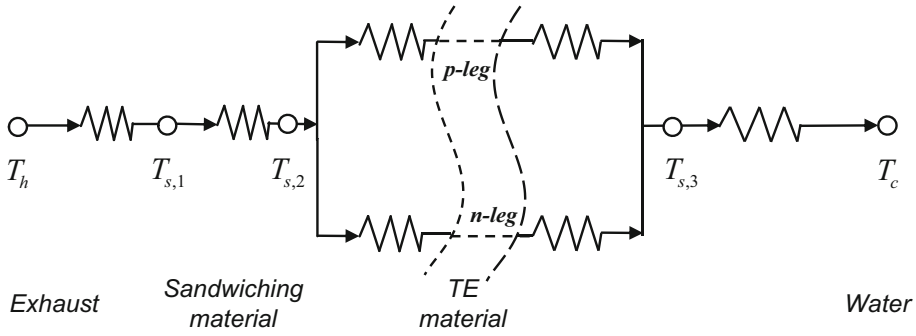

Fig. 4. The equivalent heat network of the TEG module.

Table I. The parameters of the water and the exhaust

Parameters	Symbol	Value	Symbol	Value
Medium	c	Water	h	Exhaust
Mass flow (kg/s)	$\dot{m}_c$	0.1355	$\dot{m}_h$	0.4627
Density (kg/m^3)	ρ_c	1105	ρ_h	0.667
Specific heat capacity (J/(kg K)	c_c	4181	c_h	1125
Heat convection coefficient (Wm^{-2} K^{-1})	h_c	3602	h_h	825.3
Height of cooling flow (m)	H_c	0.01	H_h	0.02

Table II. The parameters of the TE material and the sandwiching material

Parameters	Symbol	Value	Symbol	Value
Medium	w	Bi_2Te_3	m	BeO ceramic
Density (kg/m^{-3})	ρ_w	3000	ρ_m	2900
Specific heat (J/(kg K))	c_w	400	c_m	1030
Heat conductivity coefficient (Wm^{-1} K^{-1})	k_w	1.413	k_m	240
Width of material (m)	W	0.2	0.2	0.2
Length of material (m)	L	0.4	0.4	0.4
Thickness of material (m)	H_w	0.005	H_m	0.005
Contact heat convection coefficient (Wm^{-2} K^{-1})	–	–	h_m	3e + 4

thermal resistance was neglected on the contact surface of the materials. With the disparate physical properties, the temperature divisions in the TE material and the sandwiching material are discrepant. The solution of the contact surface temperature will be decided by both materials' properties, while the temperature distribution in the composite wall has been studied.[30–32] Assuming that the middle layer is in perfect contact, the temperature of the contact surface will be decided by both materials' properties. The conceptual diagram of the analysis model in the y direction is demonstrated in Fig. 5.

The central difference form of the partial differentiation of space is approximatively converted as follows:

$$\frac{\partial^2 T}{\partial y^2} = \frac{T_{i-1,j} - 2T_{i,j} + T_{i+1,j}}{\Delta y^2} \tag{20}$$

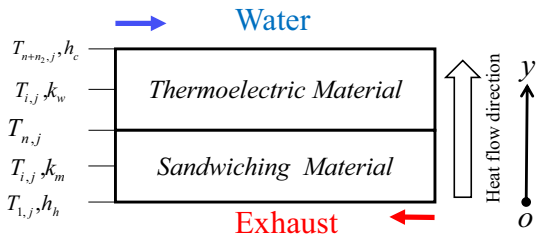

Fig. 5. The simplified physical model in the y direction.

The forward difference form of the partial differentiation of time is approximatively expressed as follows:

$$\frac{\partial T}{\partial t} = \frac{T_{i,j+1} - T_{i,j}}{\Delta t} \tag{21}$$

Then

$$\frac{T_{i-1,j}-2T_{i,j}+T_{i+1,j}}{\Delta y^2}=\frac{1}{\alpha_{\mathrm{m}}}\frac{T_{i,j+1}-T_{i,j}}{\Delta t} \tag{22}$$

$$T_{i,j+1}=c_1(T_{i-1,j}+T_{i+1,j})+(1-2c_1)T_{i,j} \tag{23}$$

$$\frac{T_{i-1,j}-2T_{i,j}+T_{i+1,j}}{\Delta y^2}=\frac{1}{\alpha_{\mathrm{w}}}\frac{T_{i,j+1}-T_{i,j}}{\Delta t} \tag{24}$$

$$T_{i,j+1}=c_2(T_{i-1,j}+T_{i+1,j})+(1-2c_2)T_{i,j} \tag{25}$$

where $c = \alpha\Delta t/\Delta y^2$, c_1, and c_2 are calculated by the physical properties of the sandwiching material and the TE material, respectively.

In the contact surface, the heat flux density is equivalent in the TE material and the sandwiching material.

$$-k_{\mathrm{m}}\frac{\partial T}{\partial y}\Big|_{y=H_{\mathrm{m}}}=-k_{\mathrm{w}}\frac{\partial T}{\partial y}\Big|_{y=H_{\mathrm{m}}} \tag{26}$$

Replacing the partial differentiation of space with the backward difference and forward difference, respectively, the equation can be expressed as:

$$-k_{\mathrm{m}}\frac{T_{n,j+1}-T_{n-1,j+1}}{\Delta y}=-k_{\mathrm{w}}\frac{T_{n+1,j+1}-T_{n,j+1}}{\Delta y} \tag{27}$$

$$T_{n,j+1}=\frac{k_{\mathrm{m}}}{k_{\mathrm{m}}+k_{\mathrm{w}}}T_{n-1,j+1}+\frac{k_{\mathrm{w}}}{k_{\mathrm{m}}+k_{\mathrm{w}}}T_{n+1,j+1} \tag{28}$$

According to Eqs. 23 and 25, the temperature of the nodes at time $(j + 1)$ in different materials can be calculated by:

$$T_{n-1,j+1}=c_1(T_{n-2,j}+T_{n,j})+(1-2c_1)T_{n-1,j} \tag{29}$$

$$T_{n+1,j+1}=c_2(T_{n+2,j}+T_{n,j})+(1-2c_2)T_{n+1,j} \tag{30}$$

According to Eqs. 28–30, $T_{n,j+1}$ can be derived as:

$$\begin{aligned}T_{n,j+1}=&\frac{k_{\mathrm{m}}c_1}{k_{\mathrm{m}}+k_{\mathrm{w}}}T_{n-2,j}+\frac{k_{\mathrm{m}}(1-2c_1)}{k_{\mathrm{m}}+k_{\mathrm{w}}}T_{n-1,j}\\&+\left[\frac{k_{\mathrm{m}}c_1}{k_{\mathrm{m}}+k_{\mathrm{w}}}+\frac{k_{\mathrm{w}}c_2)}{k_{\mathrm{m}}+k_{\mathrm{w}}}\right]T_{n,j}\\&+\frac{k_{\mathrm{w}}(1-2c_2)}{k_{\mathrm{m}}+k_{\mathrm{w}}}T_{n+1,j}+\frac{k_{\mathrm{w}}c_2}{k_{\mathrm{m}}+k_{\mathrm{w}}}T_{n+2,j}\end{aligned} \tag{31}$$

In the contact surface of the exhaust and the sandwiching material, the heat flux density can be transformed into the following forms with the central difference method.

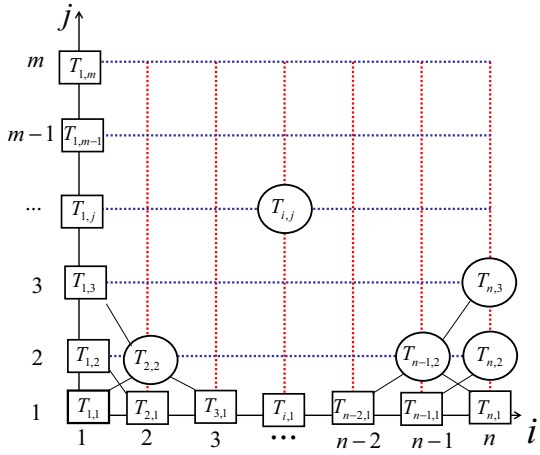

Fig. 6. Running diagram with the boundary condition and initial condition.

$$-k_{\mathrm{m}}\frac{\partial T}{\partial y}\Big|_{y=0}=h_{\mathrm{h}}[T_{\mathrm{h}}(x,t)-T(0,t)] \tag{32}$$

$$\frac{T_{2,j}-T_{0,j}}{2\Delta y}=-\frac{h_{\mathrm{h}}}{k_{\mathrm{m}}}[T_{\mathrm{h}}(x,j)-T_{1,j}] \tag{33}$$

Then

$$T_{0,j}=T_{2,j}+2\Delta y\frac{h_{\mathrm{h}}}{k_{\mathrm{m}}}[T_{\mathrm{h}}(x,j)-T_{1,j}] \tag{34}$$

$$T_{1,j+1}=c(T_{0,j}+T_{2,j})+(1-2c)T_{1,j} \tag{35}$$

$$\begin{aligned}T_{1,j+1}=&T_{1,j}\left(-2c\Delta y\frac{h_{\mathrm{h}}}{k_{\mathrm{m}}}-2c+1\right)+T_{2,j}(2c)\\&+2c\Delta y\frac{h_{\mathrm{h}}}{k_{\mathrm{m}}}T_h(x,j)\end{aligned} \tag{36}$$

Similarly, in the contact surface of the water and the TE material, the heat flux density can be exhibited as:

$$-k_{\mathrm{w}}\frac{\partial T}{\partial y}\Big|_{y=L}=h_{\mathrm{c}}[T(L,t)-T_{\mathrm{c}}(x,t)] \tag{37}$$

$$\frac{T_{n+n_2+1,j}-T_{n+n_2-1,j}}{2\Delta y}=-\frac{h_{\mathrm{c}}}{k_{\mathrm{w}}}[T_{n+n_2,j}-T_{\mathrm{c}}(x,j)] \tag{38}$$

Then

$$T_{n+n_2+1,j}=T_{n+n_2-1,j}-2\Delta y\frac{h_{\mathrm{c}}}{k_{\mathrm{w}}}[T_{n+n_2,j}-T_{\mathrm{c}}(x,j)] \tag{39}$$

$$T_{n+n_2,j+1}=c(T_{n+n_2-1,j}+T_{n+n_2+1,j})+(1-2c)T_{n+n_2,j} \tag{40}$$

$$T_{n+n_2,j+1} = T_{n+n_2,j}\left(-2c\Delta y\frac{h_c}{k_w} - 2c + 1\right) + T_{n+n_2-1,j}(2c) + 2c\Delta y\frac{h_c}{k_w}T_c(x,j) \quad (41)$$

Through the analysis of temperature iteration in the y direction, the transient temperature of the nodes $T_{1,j+1}$, $T_{i,j+1}$, $T_{n,j+1}$, and $T_{n+n2,j+1}$ can be developed by Eqs. 23, 25, 31, 36, and 41. Based on the iteration algorithms of temperature, the running diagram with the boundary condition and initial condition is explicitly portrayed in Fig. 6.

In the running diagram, i indicates the nodes of space, j indicates the nodes of time, $T_{1,j}$, $T_{n,j}$ indicate the boundary temperature in the exhaust and the water, respectively, and $T_{i,1}$ indicates the initial temperature of the space nodes in the TE material and the sandwiching material. From the diagram, the process of temperature iteration can be clearly elaborated.

RESULTS AND DISCUSSION

Analysis of the Dynamic Heat Transfer

In order to discuss the temperature reduction of the TE material along the x direction, the mathematical models of heat transfer in both directions should be calculated simultaneously. The entrance boundary conditions of the cold side and hot side are set as follows:

$$\begin{cases} T_{c,in} = 300\,\mathrm{K} \\ T_{h,in} = 1000\,\mathrm{K} \end{cases} \quad (42)$$

Through the state–space block of Matlab/Simulink, the state variables of the transient temperature of nodes in the x direction can be solved. The temperature figures of the exhaust, TE material, and water along the x direction are shown in Fig. 7.

In order to clearly illustrate the temperature variations, the temperature curves of the water and the exhaust are extracted when $x = 0$, $x = L/2$, and $x = L$. At the same time, the temperature reduction curves of the TE material in different x positions are calculated by the heat transfer model in the y direction. The analysis results of temperature variations are displayed in Fig. 8.

From the results of Fig. 8, it can be seen that the temperature of both the exhaust and the water decreases along the flowing direction. In addition, owing to the opposite flowing direction of the water and the exhaust, the temperature reduction of the TE material is almost coincident in any x position.

To analyze the temperature variations in the fluctuating boundary conditions, the inlet temperatures of the cold side and hot side are substituted as:

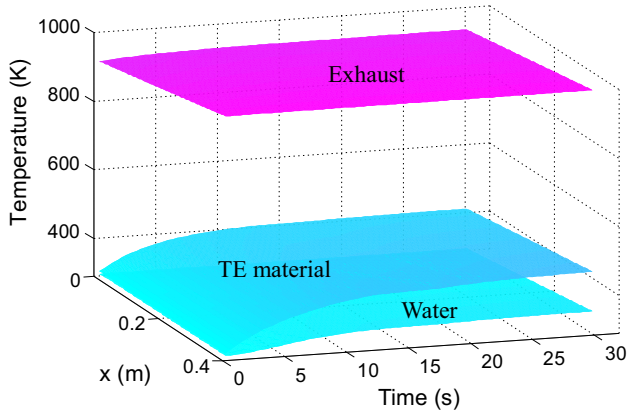

Fig. 7. The dynamic heat transfer process in time and space.

$$\begin{cases} T_{c,in} = 300 \\ T_{h,in} = 800 + 150\sin(0.1\pi t) \end{cases} \quad (43)$$

Similarly, in the case of the sinusoidal temperature fluctuations of the exhaust, the analysis results of temperature variations are shown in Fig. 9.

From the results of Fig. 9, the temperature of both the exhaust and the water decreases along the flowing direction. At the beginning of 30 s, the obvious difference of the temperature reduction of the TE material exists in different x positions, resulting from the setting of the initial temperature of the nodes. After 30 s, the temperature reduction is almost coincident along the time in the x position. Based on the analysis of heat transfer of the TE material, the temperature reduction along the x direction is substantially equivalent, which can ensure the uniformity of the temperature differences of the thermoelectric module.

Analysis of the Fluctuation Frequency of Exhaust Temperature

In order to find the relationship between the temperature of the exhaust and the TE material hot side, the fluctuation frequency of the exhaust temperature is analyzed as one of the influencing factors. Considering the different conditions of the temperature fluctuation, the inlet temperature of the exhaust with different frequencies is set as follows.

$$T_{h,in} = 800 + 150\sin(2\pi f t) \quad (44)$$

The fluctuation frequencies of the inlet temperature of the exhaust are replaced by 0.02 Hz, 0.04 Hz, 0.08 Hz, and 0.1 Hz. The temperature curves with different fluctuation frequencies are shown in Fig. 10.

The fluctuation amplitudes of the hot side of the TE material can be calculated by the difference

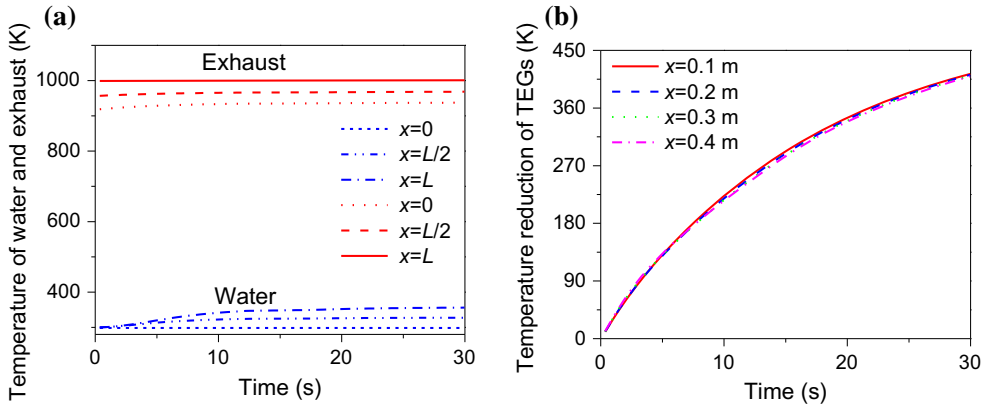

Fig. 8. Temperature curves (a) of water and exhaust and temperature reduction (b) of TEGs in the case of the static temperature fluctuations of the exhaust when $x = 0$, $x = L/2$, and $x = L$.

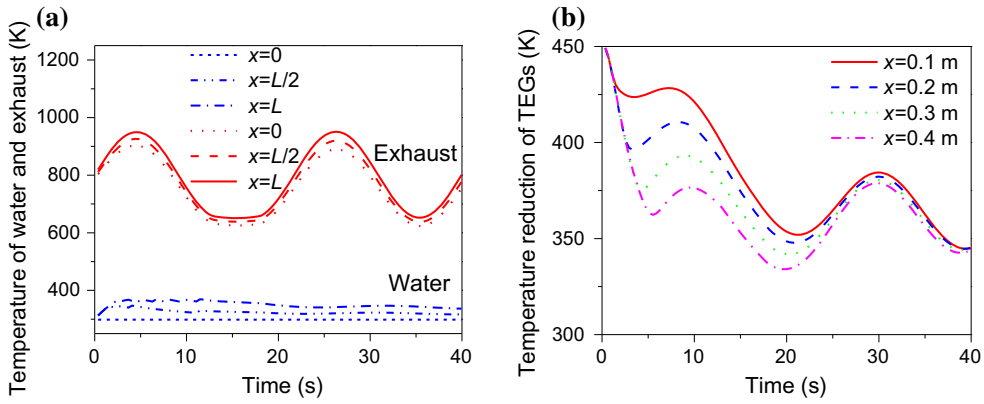

Fig. 9. Temperature curves (a) of water and exhaust and temperature reduction (b) of TEGs in the case of the sinusoidal temperature fluctuations of the exhaust when $x = 0$, $x = L/2$, and $x = L$.

between pthe eak and valley values at different frequencies, which can manifest the delay characteristic of the sandwiching material. The relationship between the temperature fluctuation amplitude and the fluctuation frequency is shown in Fig. 11. With the increasing fluctuation frequency higher than 0.01 Hz, the fluctuation amplitude obviously declines. It can be seen that the delay characteristic of the sandwiching material is more visible when the fluctuation frequency is higher than 0.04 Hz.

Analysis of the Thermal Physical Properties of the Sandwiching Material

Owning to the special position of the sandwiching material between the TE material and the exhaust, the steady temperature distribution in the y direction is decided by the thermal conductivity according to Fourier's law. In order to analyze the relationship between the thermal physical properties of the sandwiching material andthe hot side temperature of the TE material, the sandwiching material is replaced by stainless steel, BeO ceramic, and Al_2O_3 ceramic, respectively. The three kinds of materials belong to the refractory material all possess higher mechanical strength. The thermal physical properties of the different materials are shown in Table III.

On the foundation of the inlet temperature of the exhaust and the water, the hot side temperature of the TE material can be calculated. The analyzing conditions of the inlet temperature of the exhaust are divided into the sine ($f = 0.1$ Hz) and NEDC test conditions, which are shown in Fig. 12. In the NEDC urban driving conditions, a period of 200 s of the exhaust temperature is extracted as the inlet boundary condition.

From the analysis results, it can be seen the temperature fluctuation amplitude of the hot side of the TE material is less than the fluctuation of the exhaust in both conditions. In addition, the hot side of the TE material has the largest temperature reduction when the stainless steel is chosen as the sandwiching material, which can be attributed to the lower thermal conductivity of stainless steel.

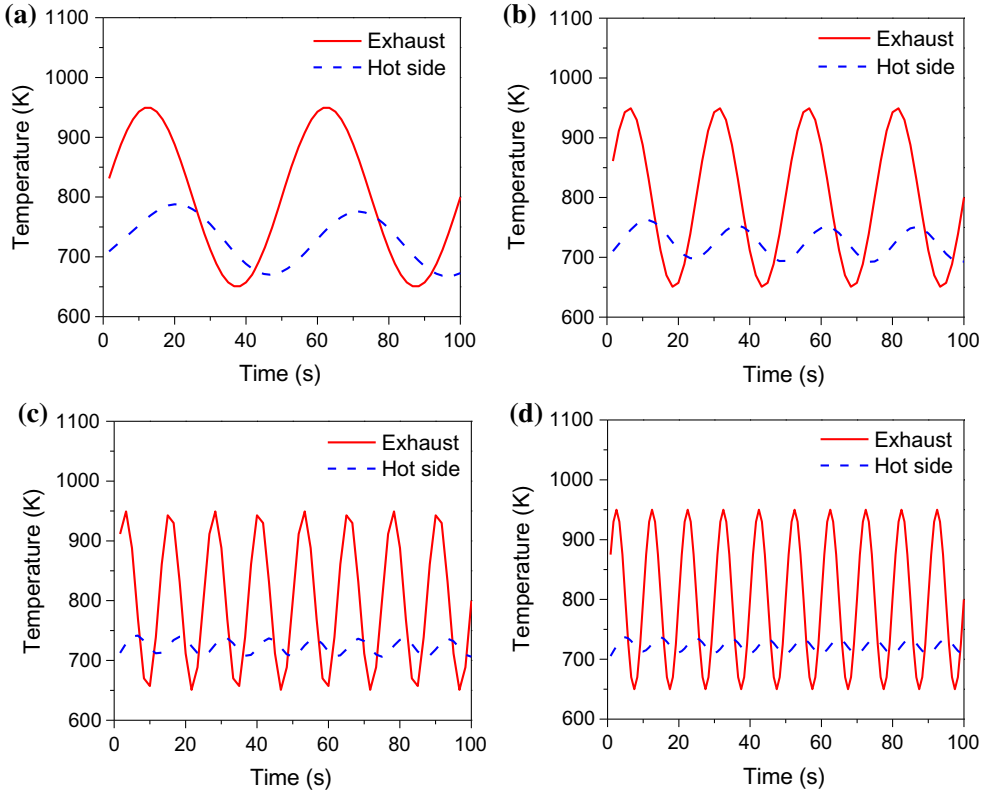

Fig. 10. The temperature curves with different fluctuation frequencies of 0.02 Hz (a), 0.04 Hz (b), 0.08 Hz (c), and 0.1 Hz (d) of the exhaust.

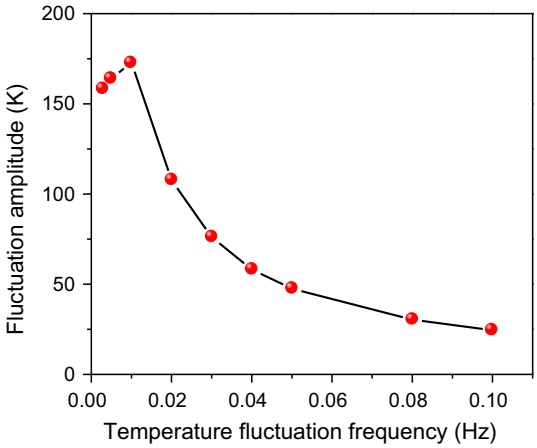

Fig. 11. The relationship between the temperature fluctuation amplitude and frequency.

To discover the influencing factors of the fluctuation amplitude of the hot side temperature of the TE material, the sandwiching materials with different thermal diffusion coefficients and thermal conductivities have been analyzed. In Fig. 13, $k_{m1} = 10$ $Wm^{-1} K^{-1}$, $k_{m2} = 50$ $Wm^{-1} K^{-1}$, $k_{m3} = 100$ $Wm^{-1} K^{-1}$, $k_{m4} = 200$ $Wm^{-1} K^{-1}$, and $k_{m5} = 300$ $Wm^{-1} K^{-1}$. With the fluctuation frequency of 0.05 Hz, the inlet temperature of the exhaust is set as follows.

$$T_{h,in} = 800 + 150 \sin(0.1\pi t) \quad (45)$$

It can be see that the lower thermal diffusion coefficient and higher thermal conductivity of the sandwiching material result in the lower temperature fluctuation amplitude which benefits the temperature stability of the hot side of the TE material.

Analysis of the Sandwiching Material Thickness

In order to analyze the relationship between the thickness of the sandwiching material and the hot side temperature of the TE material, the sandwiching material is replaced by stainless steel.

The conditions of the inlet temperature ofthe exhaust are divided into sine ($f = 0.1$ Hz) and NEDC test conditions, which are shown in Fig. 14.

From the sine and NEDC fluctuation conditions of the exhaust, the hot side temperature of the TE material decreases with the thickness of the sandwiching material. Furthermore, the larger the thickness of the sandwiching material, the slower the temperature fluctuation. In particular, with the acceleration or deceleration of the vehicle, the exhaust temperature suddenly changes synchronously and the larger thickness of the sandwiching material can ensure a lower temperature fluctuation. During 120–160 s in the NEDC driving

Table III. Thermal physical properties of different sandwiching materials

Materials	Density (kg/m^3)	Specific heat capacity (J/(kg K))	Thermal conductivity ($Wm^{-1} K^{-1}$)	Thermal diffusion coefficient (m^2/s)
Stainless steel	8055	480	15.1	3.9×10^{-6}
BeO ceramic	2900	1030	240	8.8×10^{-5}
AL_2O_3 ceramic	3940	780	32	1.04×10^{-5}

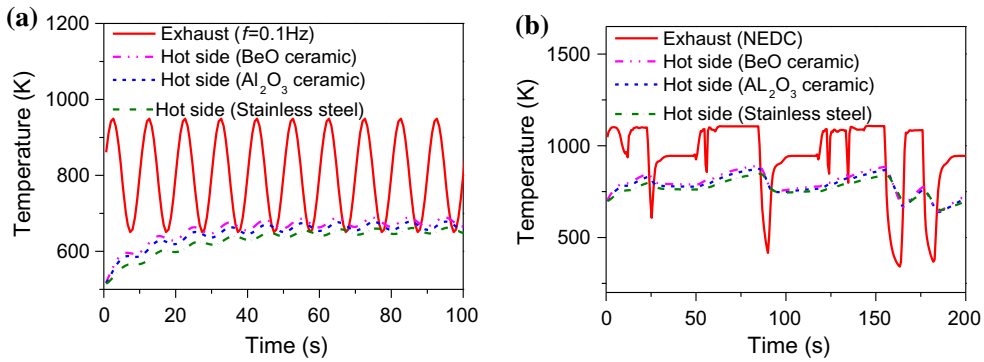

Fig. 12. The temperature curve of the hot side with different sandwiching materials in sine (a) and NEDC (b) test conditions of the exhaust temperature.

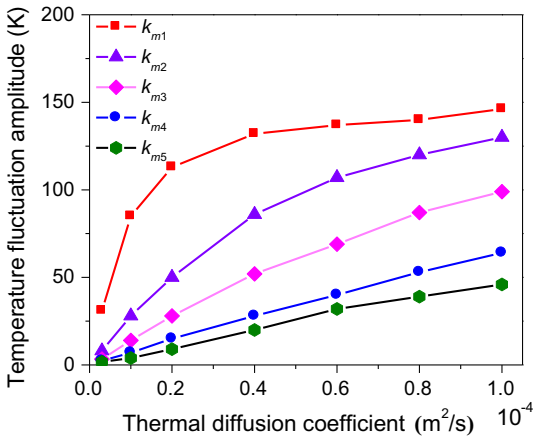

Fig. 13. The relationship between the temperature fluctuation amplitude and thermal diffusion coefficient of materials in different thermal conductivity.

conditions, the TEG with a smaller thickness of sandwiching material can generate more power. However, the smaller thickness is unfavorable for the hot side temperature stability of the TE material, and the unstable output voltage can produce adverse effects on the lifetime and work efficiency of the electronic components.[33,34] Consequently, the application of sandwiching material should consider both the generated power and the output voltage stability.

In the current work, in order to study n adequate account in the temperature loss of the TE material hot side, the pre-set parameters of temperature entering the exhaust and the water are 800 K and 300 K, individually. Figure 15 elaborates the temperature on the hot side of the TE material following the thickness and thermal conductivity of the sandwiching material. As can be seen in Fig. 15a, with the increased thickness, the temperature on the hot side of the TE material when $k_m = 10$ $Wm^{-1} K^{-1}$ declines markedly. Furthermore, with the increases of the thermal conductivity, the temperature is monotonically increased when $H_m = 2$ mm, 4 mm, and 6 mm, as shown in Fig. 15b.

In the driving conditions of vehicles, the sandwiching material with higher thermal conductivity contributes to lessen the temperature loss, which can effectually promote the output voltage of TE module. So essentially, the employment of BeO ceramic with high thermal conductivity, commendable antiknock characteristic, and excellent thermostability appears to be more efficient in the TEG system of vehicle compared with the stainless steel and AL_2O_3 ceramic. From the temperature curves in Fig. 15a, it can be forecasted the hot side temperature of TE material declines slowly with the increased thickness of BeO ceramic. In the NEDC driving conditions in Fig. 16, it can be seen the hot side temperature of TE material is the most stable when the thickness of BeO ceramic is 6 mm. During 150–170 s in NEDC driving condition, compared with the stainless steel with the thickness of 2 mm, the minimum temperature of the TE material hot side can be improved by 20.15% and the temperature reduction can increase by 115 K by using the BeO ceramic with thickness of 6 mm as the sandwiching material.

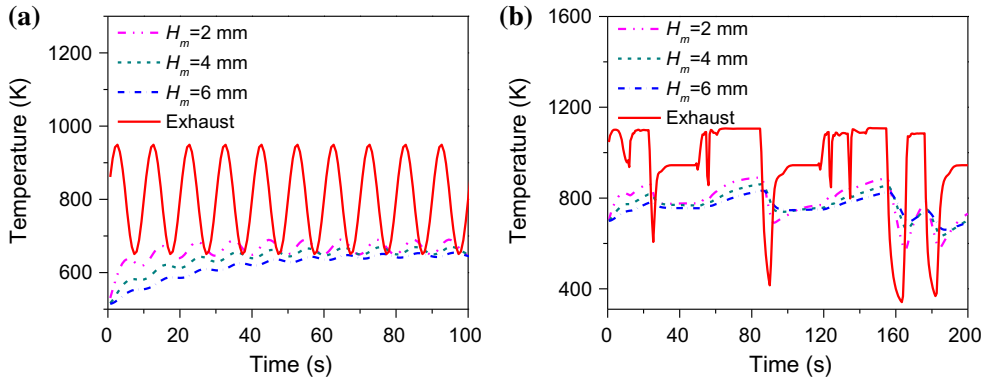

Fig. 14. The temperature curves of the hot side of the TE material with different thicknesses of sandwiching material in sine (a) and NEDC (b) test conditions of the exhaust temperature.

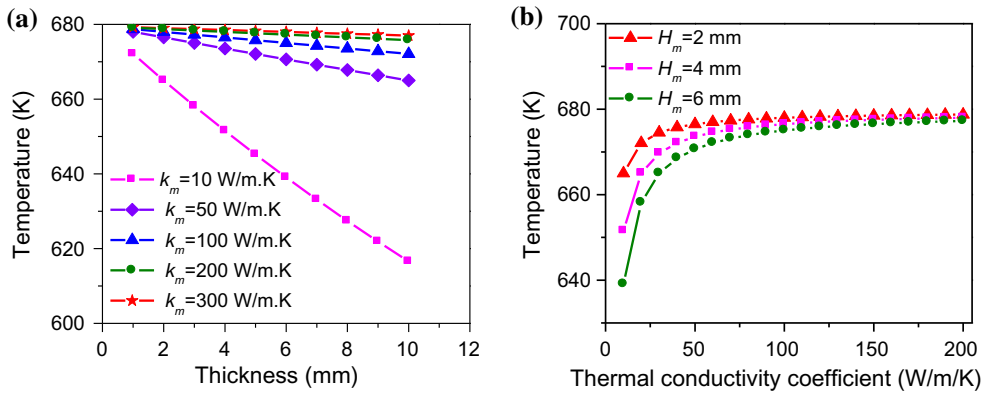

Fig. 15. The effects of the thickness (a) and thermal conductivity (b) on the hot side temperature of the TE material.

Analysis on Average Square Value of Temperature Difference

In order to weaken the adverse effects on the lifetime and work efficiency of electronic components of the TEG system, the hot side temperature stability of the TE material plays a critical role in stabilizing the output voltage. However, the effect of the sandwiching material thickness on the generating power should be compared.

The average temperature is calculated by the average integral value of the temperature function of the hot side temperature in 200 s in NEDC test conditions. Figure 17a illustrates the relationship between the average temperature and the BeO ceramic thickness in the NEDC test conditions. Figure 17b shows the minimum hot side temperature in 150–170 s with the BeO ceramic thicknesses of 2 mm and 6 mm.

In the NEDC test condition of 200 s, Fig. 17a shows that the average hot side temperature difference is only 3.01 K with the thicknesses of 2 mm and 6 mm. During 150–170 s, Fig. 17b indicates that the minimum hot side temperatures of point 1 and point 2 are, respectively, 685.70 K and 537.19 K, which shows the obvious effect of BeO ceramic thickness on the hot side temperature stability in the process of acceleration and deceleration of vehicle driving.

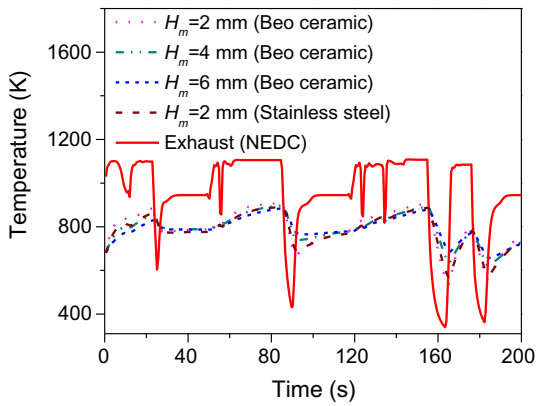

Fig. 16. The temperature curves of hot side of TE material with different thicknesses of BeO ceramic.

In the circuit with the TEG system and load, the load power is decided by the temperature difference of the TE material. Based on the Seebeck effect and Joule effect, the load power is proportional to the

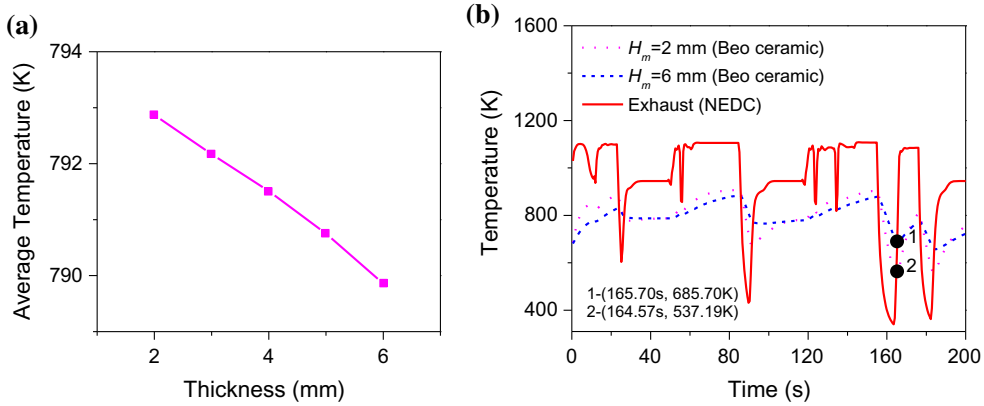

Fig. 17. (a) The relationship between the average temperature and BeO ceramic thickness in NEDC test conditions. (b) The minimum hot side temperature in 150–170 s with the BeO ceramic thicknesses of 2 mm and 6 mm.

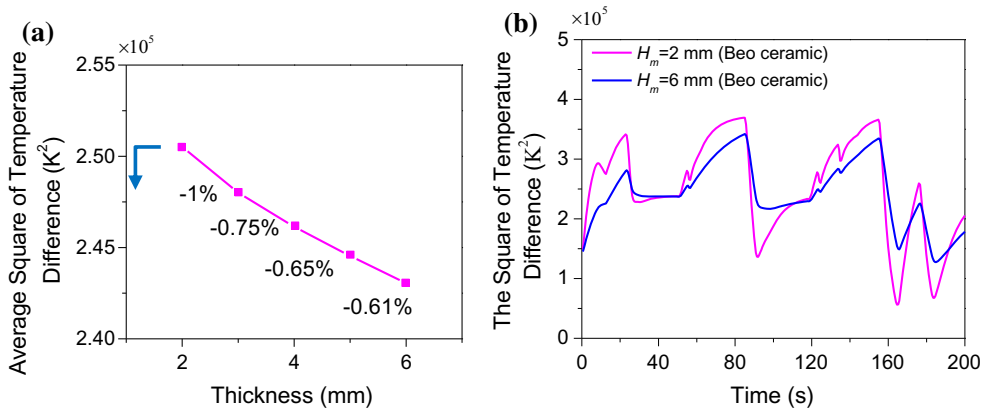

Fig. 18. (a) The relationship between the average square of temperature difference of TE material and BeO ceramic thickness in NEDC test condition. (b) The average square of temperature difference of TE material with the BeO ceramic thicknesses of 2 mm and 6 mm.

square of the temperature difference of the TE material. To clearly express the level of generation power, the average square of the TE material temperature difference is calculated by the average integral value of the square function of the TE material temperature difference in 200 s in the NEDC test condition. Figure 18a illustrates the relationship between the average square of the temperature difference of the TE material and BeO ceramic thickness in the NEDC test condition. Figure 18b shows the average square of the temperature difference of TE material in 200 s with the BeO ceramic thicknesses of 2 mm and 6 mm.

In the NEDC test condition of 200 s, Fig. 18a shows the weak effect of BeO ceramic thickness on the average square value of the temperature difference of the TE material, and the percentage value represents the decreasing level relative to the previous thickness value. In 150–170 s, Fig. 18b indicates the obvious effect on the output power stability with the thicknesses of 2 mm and 6 mm in the acceleration and deceleration processes of vehicle driving.

CONCLUSIONS

This article explores the effect factors and stability improvement methods of the TE material hot side temperature involving the fluctuation frequency of the exhaust temperature, thermal physical properties and thickness of the sandwiching material. Moreover, the average square value of the temperature difference of the TE material is proposed to evaluate the level of the generation power. The heat transfer models in transverse and longitudinal directions have been established and solved through state–space expression and temperature iteration algorithms. Based on the above analysis, we draw the following conclusions:

1. Owing to the opposite flowing direction of water and exhaust, the temperature reduction along the transverse direction is almost equivalent, which can ensure the uniformity of the temperature difference of the TE module.
2. The analysis results indicate that the properties of higher thermal conductivity, lower thermal

diffusion coefficient, and larger thickness of the sandwiching material will benefit the hot side temperature stability of the TE material. During 150–170 s in the NEDC driving condition, compared with the stainless steel with the thickness of 2 mm, the minimum temperature of the hot side of the TE material can be improved by 20.15% and the temperature reduction can increase by 115 K by using the BeO ceramic with a thickness of 6 mm as the sandwiching material.

3. The weak effect of BeO ceramic thickness on the average square value of the temperature difference of the TE material shows the small effects of sandwiching material thickness with excellent thermal conductivity on the average output power. During the 150–170 s of the NEDC test condition, the minimum hot side temperatures with BeO ceramic thicknesses of 2 mm and 6 mm are, respectively, 537.19 K and 685.70 K, which shows the obvious effect on hot side temperature stability of BeO ceramic thickness in the process of acceleration and deceleration of vehicle driving.

The larger sanwiching material thickness indicates higher heat capacity, which results in a stronger temperature delay characteristic of the TE material hot side. So, essentially, the employment of BeO ceramic can weaken the adverse effects of the frequent variation of the exhaust temperature on the lifetime and work efficiency of the electronic components of the TEG system and improve the generating power, which appears to be more efficient in the vehicle TEG system.

ACKNOWLEDGEMENTS

This work was supported by the National Natural Science Foundation of China under Grant No. 51505351 from People's Republic of China. The authors would like to show gratitude to the Hubei Key Laboratory of Advanced Technology for Automotive Components and Hubei Collaborative Innovation Center for Automotive Components Technology.

ELECTRONIC SUPPLEMENTARY MATERIAL

The online version of this article (https://doi.org/10.1007/s11664-017-5999-2) contains supplementary material, which is available to authorized users.

Open Access

REFERENCES

1. D.M. Rowe and G. Min, *J. Power Sources* 73, 193 (1998).
2. J.Q. He, M.G. Kanatzidis, and V.P. Dravid, *Mater. Today* 16, 166 (2013).
3. L.E. Bell, *Science* 321, 1457 (2008).
4. National Renewable Energy Laboratory, *Energy Technology Cost and Performance Data*. http://www.nrel.gov/analysis/tech_costs.html. Accessed 13 March 2011.
5. C.B. Vining, *Nat. Mater.* 8, 83 (2009).
6. W. He, G. Zhang, X.X. Zhang, J. Ji, G.Q. Li, and X.D. Zhao, *Appl. Energy* 143, 1 (2015).
7. H. Ohta, K. Sugiura, and K. Koumoto, *Inorg. Chem.* 47, 8429 (2008).
8. A.I. Boukai, Y. Bunimovich, J.T. Kheli, J.K. Yu, W.A.I. Goddard, and J.R. Heath, *Nature* 451, 168 (2008).
9. W. Zhu, Y. Deng, Y. Wang, S.F. Shen, and R. Gulfam, *Energy* 100, 91 (2016).
10. A.Z. Sahin and B.S. Yilbas, *Energy* 55, 899 (2013).
11. M. Zheng, G.T. Reader, and G.J. Hawley, *Energy Convers. Manag.* 45, 883 (2004).
12. T.Y. Wang, Y.J. Zhang, Z.J. Peng, and G.Q. Shu, *Renew. Sustain. Energy Rev.* 15, 2862 (2011).
13. M.A. Karri, E.F. Thacher, and B.T. Helenbrook, *Energy Convers. Manag.* 52, 1596 (2011).
14. K.M. Saqr, M.K. Mansour, and M.N. Musa, *Int. J. Automot. Technol.* 58, 155 (2008).
15. J. Han, D. Kum, and Y. Park, *Int. J. Automot. Technol.* 15, 283 (2014).
16. R. Mccarty, D. Monaghan, K. Hallinan, and B. Sanders, *J. Thermophys. Heat Transf.* 21, 505 (2007).
17. R. McCarty, K.P. Hallinan, B. Sanders, and T. Somphone, *J. Heat Transf.* 129, 749 (2006).
18. X.L. Gou, H.F. Ping, Q. Ou, H. Xiao, and S.W. Qing, *Energy Procedia* 61, 1713 (2014).
19. Z.G. Shen, S.Y. Wu, L. Xiao, and G. Yin, *Energy* 95, 367 (2016).
20. B.V.K. Reddy, M. Barry, J. Li, and M.K. Chyu, *Int. J. Therm. Sci.* 67, 53 (2013).
21. J.Y. Jang and Y.C. Tsai, *Appl. Therm. Eng.* 51, 677 (2013).
22. M. Chen, L.A. Rosendahl, T.J. Condra, and J.K. Pedersen, *IEEE Trans. Energy Convers.* 24, 112 (2009).
23. P.E. Bagnoli, C. Casarosa, E. Dallago, and M. Nardoni, *IEEE Trans. Power Electron.* 13, 1220 (1998).
24. P.G. Lau and R.J. Buist, *Proceedings ICT* (1997), pp. 563–566.
25. P. Li, L.L. Cai, P.C. Zhai, X.F. Tang, Q.J. Zhang, and M. Niino, *J. Electron. Mater.* 39, 1522 (2010).
26. D. Kraemer, K. Mcenaney, M. Chiesa, and G. Chen, *Sol. Energy* 86, 1338 (2012).
27. F.K. Meng, L.G. Chen, and F.R. Sun, *Energy* 36, 3513 (2011).
28. H. Xiao, X.L. Gou, and S.W. Yang, *J. Electron. Mater.* 40, 1195 (2011).

29. Y.Y. Hsiao, W.C. Chang, and S.L. Chen, *Energy* 35, 1447 (2010).
30. M. Torabi and K.L. Zhang, *Energy Convers. Manag.* 89, 12 (2015).
31. A. Aziz and W.A. Khan, *Energy* 36, 6195 (2011).
32. M. Li and A.C.K. Lai, *Int. J. Heat Mass Transf.* 60, 549 (2013).
33. P. Kundur, J. Paserba, V. Ajjarapu, G. Andersson, A. Bose, C. Canizares, N. Hatziargyriou, D. Hill, A.M. Stankovic, C. Taylor, T.V. Cutsem, and V. Vittal, *IEEE Trans. Power Syst.* 19, 1387 (2004).
34. P. Kundur, J. Paserba, and S. Vitet, *CIGRE/IEEE PES International Symposium Quality and Security of Electric Power Delivery Systems* (2003), pp. 1–4.